Magneto-electric Aharonov–Bohm effect in metal rings

Alexander van Oudenaarden, Michel H. Devoret*, Yu. V. Nazarov & J. E. Mooij

Department of Applied Physics and DIMES, Delft Univesity of Technology, Lorentzweg 1, 2628 CJ Delft, The Netherlands
** Permanent address: Service de Physique de l'Etat Condensé, CEA-Saclay, F-91191, Gif-sur-Yvette, France.*

The quantum-mechanical phase of the wavefunction of an electron can be changed by electromagnetic potentials, as was predicted by Aharonov and Bohm[1] in 1959. Experiments on propagating electron waves in vacuum have revealed both the magnetic[2–4] and electrostatic[5] Aharonov–Bohm effect. Surprisingly, the magnetic effect was also observed in micrometre-sized metal rings[6–8], demonstrating that electrons keep their phase coherence in such samples despite their diffusive motion. The search for the electrostatic contribution to the electron phase in these metal rings[9,10] was hindered by the high conductivity of metal, which makes it difficult to apply a well defined voltage difference across the ring. Here we report measurements of quantum interference of electrons in metal rings that are interrupted by two small tunnel junctions. In these systems, a well defined voltage difference between the two parts of the ring can be applied. Using these rings we simultaneously explore the influence of magnetic and electrostatic potentials on the Aharonov–Bohm quantum-interference effect, and we demonstrate that these two potentials play interchangeable roles.

To determine the combined influence of electrostatic and magnetic potentials on the quantum interference of electron waves, we consider the model shown in Fig. 1a and b. A metallic ring is interrupted by two tunnel barriers denoted by the black regions in Fig. 1b. Because the resistance of these tunnel barriers is much larger than the resistance of the metallic part, a well defined potential V can be applied across the two halves of the ring. Electric transport occurs because electrons can tunnel from an occupied state in the left half to an empty state in the right half, as shown in Fig. 1a. This process is equivalent to the creation of an electron–hole pair during a tunnel event. After tunnelling, the electron and the hole start to diffuse in the right and left halves of the ring, respectively. Because the transport is diffusive, the electron and hole have a finite probability of recombining at the other tunnel barrier as shown in Fig. 1b. Only those trajectories in which the electron and hole trajectories form a closed loop circling the ring are sensitive to the magnetic field through the ring. At the moment of recombination, the phase difference $\Delta\phi_B$ between the electron and hole due to the magnetic field B is $2\pi eBS/h$ (where e is the electron charge, h is Planck's constant, and S is the area of the ring). This results in alternating constructive and destructive interference between the electron and hole wave as a function of B, with a period $h/(eS)$. This effect has analogies with the modulation of the Cooper pair current with period $h/(2eS)$ in a superconducting ring interrupted by tunnel junctions (a superconducting quantum interference device, SQUID)[11,12]. But in the case of the SQUID the effect results from collective Cooper pair tunnelling (the Josephson effect), whereas here the interference takes place at the single electron level. Because of the voltage difference, the electron and hole have different energies with respect to the Fermi level in both halves of our device. The sum of the energy of the hole ϵ_h and the electron ϵ_e

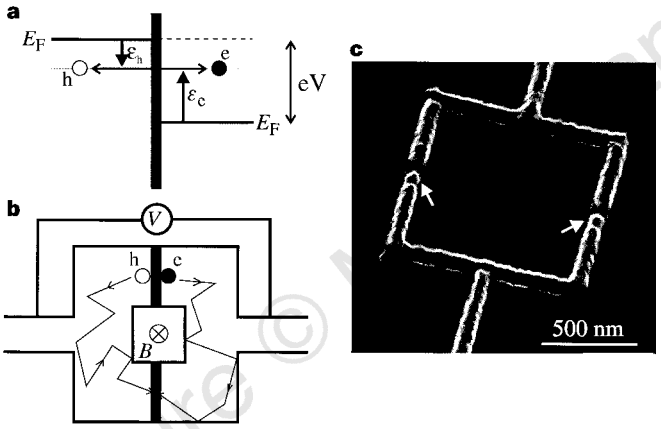

Figure 1 Quantum interference of electron–hole pair in mesoscopic ring. **a**, Energy diagram modelling a tunnelling process. At the moment of tunnelling, an electron (e) with energy ϵ_e is injected into the right part of the sample leaving a hole (h) with energy ϵ_h in the left part. **b**, Typical electron–hole trajectories which are sensitive to an Aharonov–Bohm flux. At the moment of a tunnel event an electron–hole pair is created. The hole and the electron diffuse separately to the other tunnel barrier where they recombine and interfere. The interference of the electron and hole wave is both sensitive to a magnetic field B piercing the ring (magnetic Aharonov–Bohm effect) and a voltage V across the ring (electrostatic Aharonov–Bohm effect). **c**, Scanning electron microscope image of the Aharonov–Bohm ring which is interrupted by two small tunnel junctions. The sample consists of a 0.9 μm × 0.9 μm square loop. The width of the arms of the loop is 60 nm. The loop is interrupted by two small tunnel junctions of 60 × 60 nm^2. The average distance L between the tunnel barriers is 1.6 μm. The mask of the loop was defined by electron beam lithography. The junctions were fabricated in three strips. First, a 25-nm-thick aluminium layer was deposited at an angle with respect to the oxidized Si substrate. Second, the aluminium was oxidized to form the insulating tunnel barriers. Finally, a second 40-nm-thick aluminium layer was deposited at another angle. The tunnel junctions are denoted by the arrows. By determining the overlap area of the different junctions, we conclude that the tunnelling conductances do not differ by more than 10%. This is confirmed by critical current measurements in the superconducting state, in which the sample operates as a SQUID. The tunnel conductance G_T of each junction is 55 ± 5 μS, which is about four orders of magnitude smaller than the conductance of the metallic part of the ring.

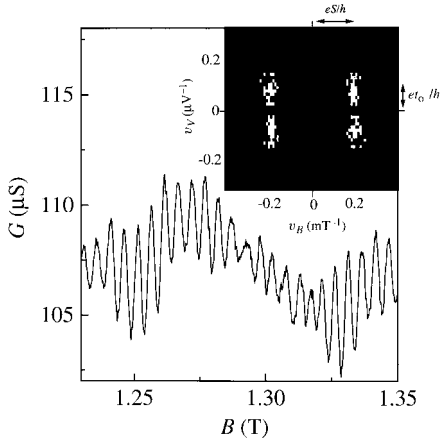

Figure 2 Conductance G versus magnetic field B at $T = 20$ mK and $V = 500$ μV. Aharonov–Bohm oscillations with a period $B_{AB} = 5$ mT are observed as a function of B. This period is in agreement with the magnetic field of 5.3 mT which is needed to add a flux quantum h/e to the average area $S = 0.75$ μm^2 enclosed by the ring. In the inset, the Fourier power spectrum is shown as a function of the magnetic and electric 'frequencies' ν_B and ν_V. The lighter the grey scale the larger the Fourier power. The magnetic and electric field modulation of G_{AB} manifests itself as peaks around ±0.2 mT^{-1} and ±0.1 μV^{-1}, respectively.

equals eV (Fig. 1a). Owing to this energy difference, the electron–hole pair accumulates an electrostatic phase difference $\Delta\phi_V = 2\pi eVt/h$, where t is the time the electron and hole spend in their respective parts of the ring before they recombine. Because electron motion is diffusive there is not one unique time, but rather a distribution of times with an average value $t_0 = L^2/D$ where L is the distance along the ring between the two tunnel barriers and D is the diffusion coefficient. The electrostatic interference results in an alternating constructive and destructive interference as a function of V with a period $h/(et_0)$. Experimentally, one can explore both the magnetic and electrostatic quantum interference effect by measuring the Aharonov–Bohm flux-dependent part G_{AB} of the conductance. The magnetic field B and the bias voltage V have an equivalent effect on G_{AB}. Changing the magnetic field at fixed V leads to a periodically oscillating G_{AB} with a period which is solely defined by the geometry of the ring. Measuring the conductance as a function of V at fixed B results in a periodically oscillating G_{AB} with an average period which is determined by t_0. In other words, by exploring the voltage dependence of G_{AB}, t_0 is measured experimentally. In the ballistic regime related interference experiments[13] have been performed in which one of the arms of the Aharonov–Bohm ring was interrupted by a quantum dot. But the relevant interference processes in such systems, where the number of electrons in the dot is changing, differ significantly from the interference in the ring we consider here.

To investigate the combined role of magnetic and electrostatic potentials we designed the sample shown in Fig. 1c. The differential conductance G at a voltage V and magnetic field B was measured using a lock-in technique. Details of the measurement set-up are given in ref. 14. All measurements were performed at $B > 1$ T to drive the aluminium loop into the normal state. At those fields time-reversal symmetry is broken, and effects related to this symmetry can be neglected. In Fig. 2 the conductance G is plotted as a function of B at a bias voltage $V = 500\,\mu$V and a temperature $T = 20$ mK. Clear periodic oscillations of the conductance are observed with a period of 5 mT, which is in good agreement with the predicted period for h/e oscillations. The relative amplitude of the Aharonov–Bohm oscillations at $V = 500\,\mu$V is ~5%, which is considerably larger than the results obtained for uniform rings[6–10]. The magnetic field not only pierces the hole of the loop, but also penetrates the arms of the loop in contrast to the ideal geometry proposed by Aharonov and Bohm[1]. This gives rise to aperiodic conductance fluctuations[14], clearly visible in Fig. 2 as the slowly varying background on top of the Aharonov–Bohm oscillations. Because of the large difference in magnetic field scales, it is possible to filter out the aperiodic conductance fluctuations using Fourier analysis. In this way we can extract (from the conductance G) the Aharonov–Bohm conductance G_{AB}, which we would measure if the field was applied only inside the ring. The Fourier power spectrum of G_{AB} with respect to B and V is shown in Fig. 2 inset.

Figure 3 shows how the Aharonov–Bohm conductance G_{AB} evolves when the bias voltage is changed. The voltage increment between two successive traces is 0.48 μV. Trace a in Fig. 3 denotes a minimum of the Aharonov–Bohm conductance at $V = 519\,\mu$V. When the voltage is decreased by 2.5 μV (trace b) the Aharonov–Bohm oscillations have almost vanished. A further decrease of the voltage by 2.5 μV (trace c) leads again to an increase of the oscillations. However, the minimum near $B = 1.032$ T for $V = 519\,\mu$V (trace a) turned into a maximum at $V = 514\,\mu$V (trace c). This observation unambiguously demonstrates the symmetry between the magnetic and the electrostatic Aharonov–Bohm effect. A maximum G_{AB} (constructive electron–hole interference) is turned into a minimum G_{AB} (destructive electron–hole interference) either by increasing the magnetic field by 2.5 mT or by increasing the voltage by 5 μV. This symmetry is also reflected in the Fourier power spectrum (Fig. 2 inset) by the peaks around $\pm 0.2\,\mathrm{mT}^{-1}$ and $\pm 0.1\,\mu\mathrm{V}^{-1}$.

To obtain a more quantitative analysis, we calculated the correlation function $C(\Delta B, \Delta V) = \langle G_{AB}(B, V) G_{AB}(B + \Delta B, V + \Delta V)\rangle$, where the angle brackets denote an ensemble average. The quantity is shown in Fig. 4. The squares in Fig. 4 denote the experimental $C(\Delta B, \Delta V = 0)$. Its oscillatory behaviour is again the manifestation of the magnetic Aharonov–Bohm effect (we denote the period by B_{AB}). The triangles in Fig. 4 denote the experimental cross-correlation

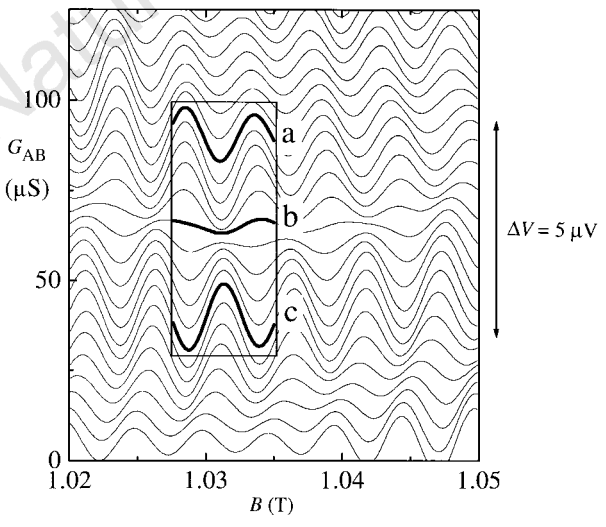

Figure 3 Aharonov–Bohm conductance as a function of magnetic field B at $T = 20$ mK for bias voltages separated by 0.48 μV. The traces have been offset by 5 μS with respect to the conductance-axis for clarity. The Aharonov–Bohm conductance G_{AB} has been extracted from G by rejecting the Fourier components of G for magnetic frequencies smaller than $0.1\,\mathrm{mT}^{-1}$. The bold traces a–c in the rectangular box show an example of the combined manifestation of the magnetic and electrostatic Aharonov–Bohm effect.

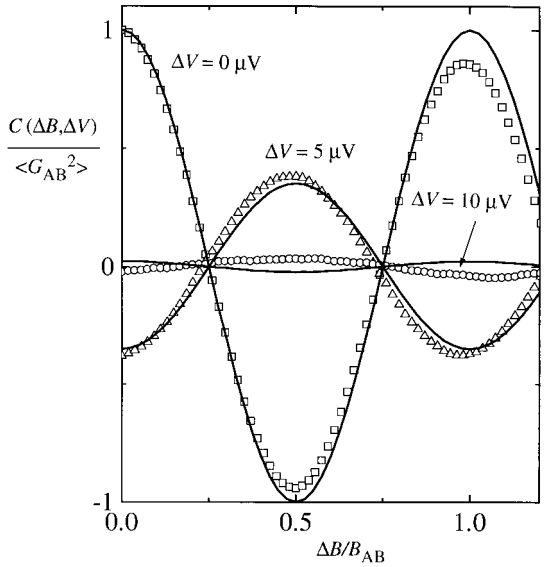

Figure 4 Normalized correlation function versus $\Delta B/B_{AB}$ at $T = 20$ mK. The correlation function $C(\Delta B, \Delta V) = \langle G_{AB}(B, V) G_{AB}(B + \Delta B, V + \Delta V)\rangle$ has been normalized to the variance $C(0, 0) = \langle G_{AB}^2\rangle$. Squares, triangles and circles correspond to $\Delta V = 0$, 5 and 10 μV, respectively. The correlation functions are calculated from a total data set consisting of 350 conductance traces as a function of B between 1.0 and 1.1 T or 2.0 and 2.1 T. These traces are measured at different voltages in the range 395–533 μV. The theoretical correlation function depends only on two parameters: t_0 and τ_ϕ, which is the time during which an electron–hole pair preserves its phase memory. A close agreement between the experimental results and theory (full lines) is found for $t_o = 300$ ps and $\tau_\phi = 300$ ps. These values are consistent with previous experiments[14].

function between two traces which are measured at bias voltages which differ by 5 μV (for example, trace a and c in Fig. 3). The correlation is maximum at $\Delta B = \frac{1}{2}B_{AB}$; this means that by increasing the bias voltage by 5 μV a minimum G_{AB} is turned into a maximum G_{AB}. At $\Delta V = 10\,\mu V$ (circles) the correlation is almost completely lost. The electron–hole pair cannot return to its creation point coherently. This is consistent with the absence of the $h/2e$ oscillations as a function of magnetic field (data not shown). When we compare our experimental results directly to the theory (shown as solid lines in Fig. 4) given in refs 14 and 15, close agreement is found.

These measurements demonstrate that the quantum-mechanical phase of diffusive electrons in metals is affected not only by a magnetic field, but also by an electrostatic field as predicted by Aharonov and Bohm. Whereas the period of the magnetic Aharonov–Bohm effect is given by the ratio of the magnetic flux through the ring to the flux quantum h/e, the period of the electrostatic Aharonov–Bohm effect is given by the ratio of the electrostatic 'Thouless flux' VL^2/D to h/e. This type of experiment enables one to directly measure the average diffusion and phase breaking time of electrons in metals. □

Received 1 September; accepted 11 November 1997.

1. Aharonov, Y. & Bohm, D. Significance of electromagnetic potentials in the quantum theory. *Phys. Rev.* **115,** 485–491 (1959).
2. Chambers, R. G. Shift of an electron interference pattern by enclosed magnetic flux. *Phys. Rev. Lett.* **5,** 3–5 (1960).
3. Möllensdedt, G., Schmid, H. & Lichte, H. in *Proc. 10th Int. Congress on Electron Microscopy* 433–434 (Deutschgesellschaft für Elektronen Mikroskopie, Hamburg, 1982).
4. Tonomura, A. *et al.* Observation of Aharonov-Bohm effect by electron holography. *Phys. Rev. Lett.* **48,** 1443–1446 (1982).
5. Schmid, H. in *Proc. 8th European Congress on Electron Microscopy* (eds Csanady, A., Rohlich, P. & Szabo, D.) 285–286 (Programme Committee of the 8th Eur. Congr. on Electron Microsc., Budapest, 1984).
6. Webb, R. A., Washburn, S., Umbach, C. P. & Laibowitz, R. B. Observation of h/e Aharonov-Bohm oscillations in normal-metal rings. *Phys. Rev. Lett.* **54,** 2696–2699 (1985).
7. Chandrasekhar, V., Rooks, M. J., Wind, S. & Prober, D. E. Observation of Aharonov-Bohm electron interference effects with period h/e and h/2e in individual micron-size, normal-metal rings. *Phys. Rev. Lett.* **55,** 1610–1613 (1985).
8. Datta, S. *et al.* Novel interference effects between parallel quantum wells. *Phys. Rev. Lett.* **55,** 2344–2347 (1985).
9. Washburn, S., Schmid, H., Kern, D. & Webb, R. A. Normal-metal Aharonov-Bohm effect in the presence of a transverse electric field. *Phys. Rev. Lett.* **59,** 1791–1794 (1987).
10. Washburn, S. & Webb, R. A. Quantum transport in small disordered samples from the diffusive to the ballistic regime. *Rep. Prog. Phys.* **55,** 1311–1383 (1992).
11. Barone, B. & Paternò, G. *Physics and Applications of the Josephson Effect* (Wiley, New York, 1982).
12. Likharev, K. K. *Dynamics of Josephson Junctions and Circuits* (Gordon & Breach, Philadelphia, 1986).
13. Schuster, R. *et al.* Phase measurement in a quantum dot via double-slit interference experiment. *Nature* **385,** 417–420 (1997).
14. Van Oudenaarden, A., Devoret, M. H., Visscher, E. H., Nazarov, Yu. V. & Mooij, J. E. Conductance fluctuations in a metallic wire interrupted by a tunnel junction. *Phys. Rev. Lett.* **78,** 3539–3542 (1997).
15. Nazarov, Yu. V. Aharonov-Bohm effect in the system of two tunnel junctions. *Phys. Rev. B* **47,** 2768–2774 (1993).

Acknowledgements. We thank P. W. Brouwer for discussions. This work was supported by the Dutch Foundation for Fundamental Research on Matter (FOM).

Correspondence and requests for materials should be addressed to A.v.O. (e-mail: socrates@qt.tn.tudelft.nl).

Noise-supported travelling waves in sub-excitable media

Sándor Kádár, Jichang Wang & Kenneth Showalter

Department of Chemistry, West Virginia University, Morgantown, West Virginia 26506-6045, USA

The detection of weak signals of nonlinear dynamical systems in noisy environments may improve with increasing noise, reaching an optimal level before the signal is overwhelmed by the noise. This phenomenon, known as stochastic resonance[1,2], has been characterized in electronic[3], laser[4], magnetoelastic[5], physical[6] and chemical[7] systems. Studies of stochastic resonance and noise effects in biological[8,9] and excitable dynamical systems[10–13] have attracted particular interest, because of the possibility of noise-supported signal transmission in neuronal tissue and other excitable biological media. Here we report the positive influence of noise on wave propagation in a photosensitive Belousov–Zhabotinsky[14–17] reaction. The chemical medium, which is sub-excitable and unable to support sustained wave propagation, is illuminated with light that is spatially partitioned into an array of cells in which the intensity is randomly varied. Wave propagation is enhanced with increasing noise amplitude, and sustained propagation is achieved at an optimal level. Above this level, only fragmented waves are observed.

Experiments were carried out with thin layers of silica gel in which ruthenium(II)-bipyridyl, a light-sensitive catalyst for the Belousov-Zhabotinsky (BZ) reaction, was immobilized[18]. The gel was continually bathed with fresh, catalyst-free BZ reagents in a Plexiglas reactor to maintain the system in an unvarying non-equilibrium state[19]. Gels were exposed (from below) to spatially homogeneous light transmitted from a video projector through a 460-nm bandpass filter. The light intensity was adjusted to an appropriate reference level for maintaining the system slightly below the excitability threshold (determined by the photochemical production of Br^- ion[16,20], an inhibitor of autocatalysis in the BZ reaction). The illumination field consisted of an array of square cells, with the intensity in each adjusted at equal time intervals to random values above or below the reference level. The random intensities were gaussian-distributed with the mean amplitude centred at the reference intensity.

The effects of the spatiotemporal noise on wave propagation are shown in Fig. 1, where superimposed 'snapshots' depict the evolution of a single wave segment at equal time intervals. The noise level was varied from zero in Fig. 1a, corresponding to the noise-free autonomous system, to the maximum level in Fig. 1d, which was determined by the reference intensity. A typical noise pattern is shown in Fig. 1e, where the boundary was provided by light intensity at the reference level. Waves were generated in the adjacent region, with a lower light intensity (and higher excitability), at the left-hand side. In the absence of noise, waves entering the sub-excitable region became shrinking wave segments (Fig. 1a). Below the excitability threshold, free wave ends simply recede rather than form the familiar rotating spiral waves observed in excitable media[21,22]. Propagation failure occurs when the receding wave disappears, as shown in the final frame of the overlaid images. A slight enhancement of wave propagation is observed with low-level noise (Fig. 1b), in which wave failure occurs about one frame later. At higher noise levels (Fig. 1c), the wave segment no longer shrinks but propagates through the entire medium. At still higher levels (Fig. 1d), fragmentation of the wave occurs at wave breaks induced by high-intensity perturbations.

The dependence of the signal strength on noise level and cell size is summarized in Fig. 2. The relative signal strength was defined by the size of the wave segment (number of pixels above a specified grey level) at the point of wave failure in the autonomous system relative to the size of the wave segment entering the sub-excitable region. An increase in the noise level results in an increase in the size of the wave segment passing through the detection point, reaching a maximum at an optimum noise level. Wave propagation also depends on the degree of spatial correlation of the noise, which is determined by the cell size. For a cell size (4×4 pixels) comparable to the length scale of the wave width, the optimal noise level is ~0.6 of the maximum level. The optimal noise level increases as the cell size decreases, to ~0.8 of the maximum level for cells of 2×2 pixels. No optimal level was found, within our experimental noise range, when the cell size was defined by one pixel. Related trends in spatial correlation dependence have been found in theoretical studies of stochastic resonance in excitable media[12,13].

Numerical studies of noise-supported wave propagation were carried out using the Tyson–Fife[23] scaling of the Oregonator